Turkish Journal of Electrical Engineering and Computer Sciences

Volume 24 | Number 4 Article 79

1-1-2016

A new combined method for RMS calculation based on wavelet packet and Hilbert transform

RAHMAT ALLAH HOOSHMAND

Javad Modarresi

Turkish Journal of Electrical Engineering & Computer Sciences

http://journals.tubitak.gov.tr/elektrik/

Research Article

Turk J Elec Eng & Comp Sci
(2016) 24: 3178 – 3197

doi:10.3906/elk-1404-225

A new combined method for RMS calculation based on wavelet packet and Hilbert transform

Javad MODARRESI, Rahmat-Allah HOOSHMAND*
Department of Electrical Engineering, University of Isfahan, Isfahan, Iran

Received: 13.04.2014 • **Accepted/Published Online:** 15.03.2015 • **Final Version:** 15.04.2016

Abstract: Among several methods used for calculating the root mean square (RMS) of electrical signals, Fourier and wavelet transforms are the most common approaches. The latter also has the advantage of being able to analyze both stationary and nonstationary signals. However, in the wavelet-based methods, the presence of both odd and even harmonics in the input signal causes the harmonic components not to be in the center of the extracted frequency bands and this will reduce the accuracy of the RMS calculation. In order to remove this drawback, this paper proposes a new method based on wavelet and Hilbert transforms, in which the frequency of all harmonic components is increased by half of the main frequency by using a preprocessing technique. In simulation results, the RMS value of a real signal of the steel electric arc furnace of the Esfahan Mobarakeh Steel Company is calculated by using the suggested method. The results clearly show that the accuracy of the proposed approach is better than that of conventional and grouping methods.

Key words: Even harmonics, odd harmonics, Hilbert transform, root mean square value, wavelet packet transform, electric arc furnace

1. Introduction

Nowadays, with an increase in the use of power electronic devices, electric arc furnaces (EAFs; AC and DC), and induction furnaces, odd and even harmonics are injected into power systems [1–3]. Since harmonics have adverse effects on power systems, they must be removed; however, this removal demands careful study [4–6]. For this purpose, Fourier-based methods have been proposed. Although these methods shown a very good performance, they are unsuitable for the analysis of nonstationary waveforms [7–9]. In this case, the FFT introduces serious errors due to the spectral leakage and picket fence phenomena [7]. Figure 1a shows a nonstationary current waveform of 50 Hz frequency. The current amplitude changes with time; it starts from an initial value of 10 A at t = 0 s and then the amplitude increases to 60 A at t = 0.1 s. The FFT spectrum shows a 35 A component at 50 Hz (which does not exist in the original waveform). Moreover, the FFT spectrum shows other components spread along the frequency axis; these components do not exist in the original waveform, either. The spectral leakage is very evident from Figure 1b, which causes inaccurate results.

Wavelet packet transform (WPT)-based methods have been proposed to overcome the drawbacks of the Fourier-based methods [10]. Although the computational burden of the wavelet transform is higher than that of the Fourier transform [11], the Fourier transform can only be used to analyze stationary signals. Thus, using the wavelet transform to analyze nonstationary signals is inevitable.

*Correspondence: hooshmand_r@yahoo.com

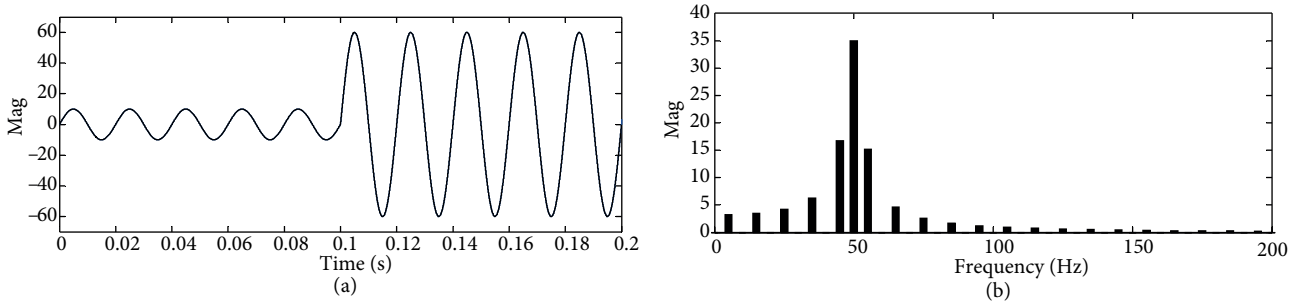

Figure 1. Nonstationary waveform: (a) time domain waveform, (b) FFT spectrum.

In wavelet-based methods, the input signal must be sampled so that the frequency of all harmonics is located in the center of extracted frequency bands to enhance the calculation accuracy. Odd harmonics frequency can be easily located in the center of extracted frequency bands if there are only odd harmonics in the signal understudy. However, this cannot be done easily for signals with both odd and even harmonics.

So far, 2 methods have been proposed for RMS value calculation by WPT. These methods are the conventional method [12–14] and grouping methods [15–19]. The conventional method assumes that only odd harmonics exist in the signal under study and so the input signal is decomposed by WPT so that the odd harmonics are located in the center of extracted frequency bands. Depending on the even harmonics' amplitude, the existence of both odd and even harmonics can affect the accuracy of RMS calculation in the conventional method since the even harmonics are located on the border of the extracted frequency bands, causing harmonic frequency interference. Moreover, the calculation of the DC component amplitude is not present in the conventional method.

The grouping method assumes that both odd and even harmonics exist in the signal under study. In this method, the input signal is decomposed by WPT so that the harmonics (both odd and even harmonics) are located on the border of the extracted frequency bands. Then the outputs of WPT are grouped to calculate the RMS values (grouping method). This method has been used properly to study harmonics, but this method is not able to calculate the fundamental RMS value accurately. The calculation of the DC component amplitude is present in the grouping method.

In this paper, a new method is proposed to calculate the RMS value. This method is a combination of the WPT and Hilbert transform. The Hilbert transform is widely used in power quality studies. For example, in [10], the input signal is first applied to a discrete Hilbert transform whose aim is to obtain a signal, orthogonal to the input signal. Then the amplitude and phase angle of the fundamental component of the input signal are obtained by the complex WPT coefficient. In the proposed method, the complex WPT coefficients are created as in [10], and then the frequency of all components is increased by half of the main frequency. This process locates each harmonic component (both odd and even harmonics) in the center of the extracted frequency bands. Thus, harmonic frequency interference does not occur in the proposed method. Moreover, the calculation of the DC component amplitude is presented in the proposed method. The proposed method can calculate the fundamental RMS value more accurately compared with the grouping method. For the arc voltage of an EAF in the early stage of charging, the percentage error of the fundamental RMS value in the proposed method and in the grouping method is 0.1078% and 45.3763%, respectively. Moreover, at a fixed sampling frequency, the number of WPT levels in the proposed method is less than in the grouping method always by one.

To examine the validity of the proposed method and make a comparative study with the conventional and

grouping methods, the EAF of the Esfahan Mobarakeh Steel Company (EMSC) in different operation conditions and a hypothetical signal were simulated by MATLAB software to consider both odd and even harmonics. The results confirm the superiority of the proposed method.

The remaining part of this paper is organized as follows: Section 2 considers the wavelet transform clarification. Section 3 examines the RMS value definition in the wavelet domain. Section 4 outlines the proposed method and its details. A case study and analysis of the results are presented in Section 5, Section 6 studies the time cost and computational burden, Section 7 examines the effect of mother wavelets, and Section 8 concludes the paper.

2. Wavelet transform

In general, wavelet theory encompasses continuous wavelet transform (CWT), discrete wavelet transform (DWT), and WPT as introduced in this section.

2.1. Continuous wavelet transform

The CWT of a continues signal ($f(t)$) at scale a and position b is computed by Eq. (1):

$$W_f(a,b) = |a|^{-\frac{1}{2}} \int_{-\infty}^{\infty} f(t)\psi^* \left(\frac{t-b}{a}\right) dt \tag{1}$$

where the symbol $*$ denotes the complex conjugate and ψ is the mother wavelet. The mother wavelet is a function of the zero average, while the limited period that is dilated by the scale parameter a and translated by b is shown in Eq. (2).

$$\psi_{a,b}(t) = |a|^{-\frac{1}{2}} \psi \left(\frac{t-b}{a}\right) a, b \in R, a \neq 0 \tag{2}$$

The signal $f(t)$ can be decomposed by Eq. (3).

$$f(t) = \frac{1}{C_\psi} \int_{-\infty}^{\infty} \int_{-\infty}^{\infty} \frac{1}{a^2} W_f(a,b)\psi \left(\frac{t-b}{a}\right) dadb \tag{3}$$

Here, $C_\psi = \int_{-\infty}^{\infty} \frac{|\psi(\omega)|^2}{\omega} d\omega < \infty$,

2.2. Discrete wavelet transform

DWT is designed by the multiresolution analysis that decomposes the input signal into various frequency bands with their width depending on sampling frequency and DWT levels. Figure 2 shows a 2-level DWT [20].

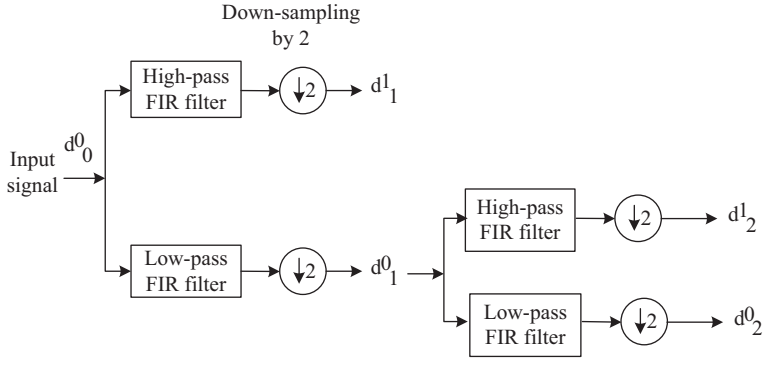

Figure 2. Two-level analysis part of the DWT.

In this figure, d_j^m is the wavelet coefficient at the decomposition level j and the frequency band m [7]. In each level, the input signal is filtered by FIR low-pass and high-pass filters and then is downsampled by 2. This process decomposes the input signal into several frequency bands with the FIR filter coefficients depending on the mother wavelet. The relationship between the sampling frequency (f_s) and the frequency band width (f_{bw}) can be expressed by [21]:

$$f_{bw} = \frac{f_s}{2^{J+1}} \tag{4}$$

where J is the total number of DWT levels.

2.3. Wavelet packet transform

WPT is a generalization of the DWT that performs a full decomposition tree. In other words, WPT decomposes the input signal into several frequency bands with the same length. Figure 3 shows the 2 decomposition level tree [22].

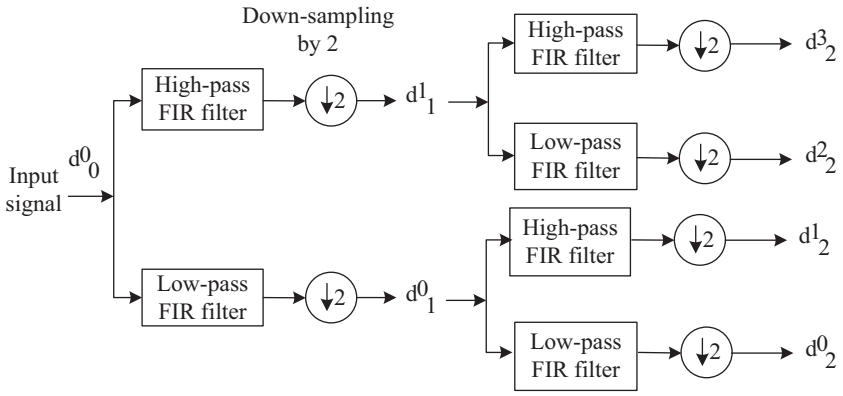

Figure 3. Structure of WPT.

In WPT, the number of the extracted frequency bands at decomposition level j (M_j) is obtained by Eq. (5).

$$M_j = 2^j \tag{5}$$

According to Eq. (5), if the total number of WPT levels is equal to J, the total number of the extracted frequency bands (M) will be equal to:

$$M = \sum_{i=1}^{J} 2^i = 2\left(2^J - 1\right) \tag{6}$$

3. RMS value definition in the wavelet domain

WPT is a time-frequency domain tool, which can be used for RMS value calculation in power systems. The input signal must be decomposed into several frequency bands for calculating the RMS value. In the time–frequency domain, the signal $v(t)$ with the 2^N sample point can be expressed by the following equation [20]:

$$v(t) = \sum_{k=0}^{2^{N-J}-1} d_j^0[k]\,\phi_{j,k}(t) + \sum_{n=1}^{2^J-1}\left(\sum_{k=0}^{2^{N-J}-1} d_j^n[k]\psi_{j,k}^n(t)\right) = v_j^0 + \sum_{n=1}^{2^J-1} v_j^n \tag{7}$$

where d_j^n is the WPT coefficient at frequency band n and decomposition level j, and v_j^n is the voltage at extracted band n and decomposition level j. Also, φ and ψ are the scaling function and the mother wavelet, respectively. The RMS value in the wavelet domain can be obtained by substituting Eq. (7) into the RMS value time domain formula. After simplification, Eq. (8) is obtained for the RMS value.

$$v_{rms} = \sqrt{\frac{1}{2^N}\sum_{k=0}^{2^{N-j}-1}\left(d_j^0[k]\right)^2 + \frac{1}{2^N}\sum_{m=1}^{2^j-1}\sum_{k=0}^{2^{N-j}-1}\left(d_j^m[k]\right)^2} \tag{8}$$

Eq. (8) is proven in Appendix A.

4. Proposed method

The proposed method calculates the RMS value by the Hilbert transform and WPT, which will be explained in the next subsection. Then the proposed method's flowchart is described in detail.

4.1. Hilbert transform

The Hilbert transform is a time-domain to time-domain transformation, which shifts the phase of a signal by $\pi/2$. Positive frequency components are shifted by $+\pi/2$ rad and negative frequency components are shifted by $-\pi/2$ rad. Applying a Hilbert transform to a signal twice in succession shifts the phases of all of the components by π rad. The Hilbert transform is defined by [22]:

$$H(v(t)) = \frac{1}{\pi}\int_{-\infty}^{\infty}\frac{v(\tau)}{t-\tau}d\tau = v(t) * \frac{1}{\pi t} \tag{9}$$

According to Eq. (9), the Hilbert transform can be considered as the convolution integral of signal $v(t)$ and $1/(\pi t)$. In this paper, the main contribution of the Hilbert transform is to shift the frequency of the input signal components by producing an orthogonal signal. The frequency shifting is necessary to locate both the odd and the even harmonics in the center of the extracted frequency bands by wavelet transform.

4.2. Proposed method flowchart

In the proposed method, the Hilbert transform of the input signal is first calculated and then an equation in a complex form is written as follows:

$$a = v(t) + jH\left(v\left(t\right)\right) \tag{10}$$

where H(v(t)) is the Hilbert transform of v(t) and j is an imaginary unit. If an exponential form of a complex number is multiplied in Eq. (10), the frequency of all the components will increase. This process is shown as in Eq. (11):

$$b = a \times e^{\pi f t j} \tag{11}$$

where f is the main frequency and t is the time. As such, the frequency of all harmonics is shifted by $f/2$ and odd and even harmonics are located in the center of the extracted frequency bands. After increasing the frequency of all the components by Eq. (11), the real part of Eq. (11) is chosen as the input signal of the WPT. This process is shown as follows:

$$d_{0,k}^0 = Real\left(b\right) \tag{12}$$

It should be noted that if the DC component exists in the input signal, the actual overall RMS value will be obtained by the following equation:

$$v_{rms} = \sqrt{A_{DC}^2 + \sum_{i=1}^{n} \frac{A_i^2}{2}} \tag{13}$$

where A_{DC} is the DC component amplitude and A_i is the ith harmonic amplitude. If the proposed method is used for the calculation of the overall RMS value, the DC component will appear as a sinusoidal wave of $f/2$ frequency. In this case, the overall RMS value will be equal to:

$$v_{rms} = \sqrt{\frac{A_{DC}^2}{2} + \sum_{i=1}^{n} \frac{A_i^2}{2}} = \sqrt{\left(\frac{A_{DC}}{\sqrt{2}}\right)^2 + \sum_{i=1}^{n} \frac{A_i^2}{2}} \tag{14}$$

Eqs. (13) and (14) do not offer the same overall RMS value. Therefore, Eq. (14) must be converted to Eq. (13). For this purpose, if the lowest extracted frequency band, which includes only the DC component, is multiplied by $\sqrt{2}$, Eq. (14) will be converted to Eq. (13). Considering the mentioned topics, the flowchart of the proposed method can be drawn as in Figure 4.

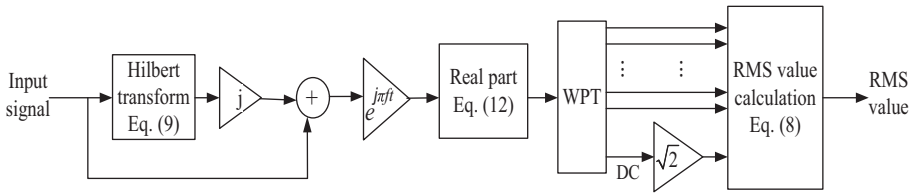

Figure 4. Proposed method's flowchart.

It should be noted that the wavelet transform is very sensitive to the end effects of the analyzed signal. The end effects are very common in processing finite-length signals [23,24]. The proposed method has been designed to calculate the RMS voltage and the current of the EAF of the EMSC in real-time. Thus, the input signal of the proposed method can be considered as an infinite signal and the end effects can be ignored. Therefore, the end effects are not considered in the proposed method.

5. Case studies

To examine the proposed method, 2 cases are evaluated by MATLAB software. The first case is the supplying network of the EAF of the EMSC, while the other case is a hypothetical signal in the MATLAB environment.

5.1. First case study (EAF of EMSC)

In this subsection, the supplying network of the EAF of the EMSC is simulated by MATLAB software in different operational conditions. The network of the EAF of the EMSC is shown in Figure 5a. The EAF is connected to the point of common coupling (PCC) through the cable, furnace transformer (T_F), and main transformer (T_S). The T_F is used to change the active input power of the arc furnace. This transformer is equipped with a tap changer located at the secondary winding to change the voltage of the furnace.

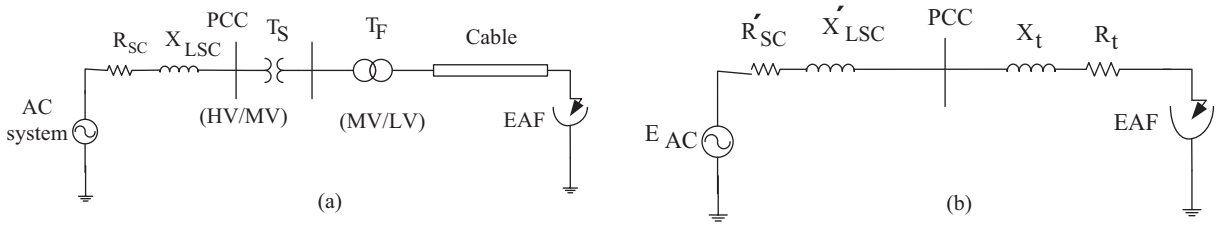

Figure 5. Supplying network of EAF: (a) single-line diagram, (b) simplified model.

The simplified model of the simulated network is shown in Figure 5b. In this figure, all the impedances have been transferred into the secondary of T_F. In the figure, $\dot{X}_{LSC}$ and $\dot{R}_{SC}$ are the short circuit reactance and the resistance at the bus PCC, respectively. X_t and R_t are the equivalent reactance and resistance of the cable, T_F and T_S. The specifications of the supplying network are given in Appendix B.

5.1.1. Load modeling of EAF model

The EAF is one of the most important furnaces for steelmaking, smelting, and refining of scrap metals. The EAF consists of a refractory-lined vessel covered with a retractable roof through which one or more graphite electrodes enter the furnace. Scrap metal is delivered to the vessel and then melted by an electric arc generated by graphite electrodes. In this subsection, 3 time-domain models of the EAF are introduced. These models are hyperbolic, exponential, and exponential-hyperbolic models.

5.1.1.1. Hyperbolic model

In this model the voltage-current characteristic (VIC) of the EAF is considered as follows [1,25,26]:

$$V_{arc}(I_{arc}) = \begin{cases} \left(V_T + \frac{C_i}{D_i + |I_{arc}|}\right) sign(I_{arc}) \frac{dI_{arc}}{dt} \geq 0 \\ \left(V_T + \frac{C_d}{D_d + |I_{arc}|}\right) sign(I_{arc}) \frac{dI_{arc}}{dt} < 0 \end{cases} \tag{15}$$

where I_{arc} and V_{arc} are the arc current and voltage of a specific phase, respectively. V_T is the magnitude of the voltage threshold that the voltage approaches as the current increases. (C_i, C_d) and (D_i, D_d) correspond to the arc power and the arc current, respectively, and they can take different values.

5.1.1.2. Exponential model

In this model, the VIC of the EAF is described as in Eq. (16) [1].

$$V_{arc}(I_{arc}) = V_T(1 - e^{-\frac{|I_{arc}|}{I_0}}) sign(I_{arc}) \tag{16}$$

In Eq. (16), a current constant (I_0) is employed to model the steepness of the positive and negative currents, and an exponential function is used to describe the VIC of the EAF.

5.1.1.3. Exponential-hyperbolic model

The exponential and hyperbolic models are traditional models and the exponential-hyperbolic model is a combination of these models. Thus, the exponential-hyperbolic model has characteristics of both hyperbolic

and exponential models. This model is defined by Eq. (17) [1]:

$$V_{arc}\left(I_{arc}\right)=\begin{cases}\left(V_T+\frac{C}{D+|I_{arc}|}\right)sign\left(I_{arc}\right)\frac{dI_{arc}}{dt}\geq 0\\ V_T\left(1-e^{-\frac{|I_{arc}|}{I_0}}\right)sign\left(I_{arc}\right)\frac{dI_{arc}}{dt}<0\end{cases} \tag{17}$$

where C and D correspond to the arc power and arc current, respectively. The exponential-hyperbolic model has the following main features [1,27,28]:

1. Modeling of the EAF with good approximation with no need for the initial conditions of the EAF.
2. Description of different operating conditions of the EAF and the power system.
3. Presentation of an efficient model with a very good approximation for the VIC.
4. Characteristics of both the hyperbolic and exponential models.

According to the mentioned features, the exponential-hyperbolic model is the best choice for EAF modeling. Thus, in this paper, the exponential-hyperbolic model has been used for EAF modeling.

Depending on the value of V_T, the EAF can work on the balanced, unbalanced, and early stages of charging [1]. In order to simulate the balanced and unbalanced conditions of the EAF, the same and different values of V_T in Eq. (17) are chosen for different phases, respectively. In addition, different values of V_T are considered for the positive and negative parts of each phase current to simulate the even harmonics with relatively high amplitude in the early stage of charging.

The V_T for the positive and negative current of the EAF of the EMSC is considered as $V_T = 200$ (positive current) and $V_T = 175$ (negative current) [1]. The greater difference between the negative and the positive currents leads to a greater amplitude of even harmonics. Thus, considering the worst condition in this paper, V_T is chosen as 180 and 220 for the negative and the positive current, respectively. The parameters employed to simulate the EAF are shown in Appendix B.

5.1.2. Frequency increase by the proposed method

As mentioned, the proposed method increases the frequency of all harmonics equal to half of the main frequency where the main frequency is 50 Hz. The frequency of V_{arc} is increased by Eq. (11) to evaluate the frequency increase by the proposed method.

V_{arc} in the early stage of charging is shown in Figure 6a. In [7], 32 samples per fundamental cycle (1920 Hz for 60 Hz) are used for power and RMS calculation by the wavelet packet transform. In this paper, 64 samples per fundamental cycle (3200 Hz for 50 Hz) are used for considering the signals with better resolution. Moreover, according to the Nyquist sampling theorem, harmonics order up to order 32 can be studied by 3200 Hz sampling frequency. On the other hand, according to Figure 6b, the amplitude of the harmonic orders greater than 32 can be neglected in comparison with low-order harmonic amplitudes. Therefore, in this paper, the sampling frequency of 3200 Hz has been used to have a tradeoff between the accuracy and time cost (high sampling frequency increases the time cost).

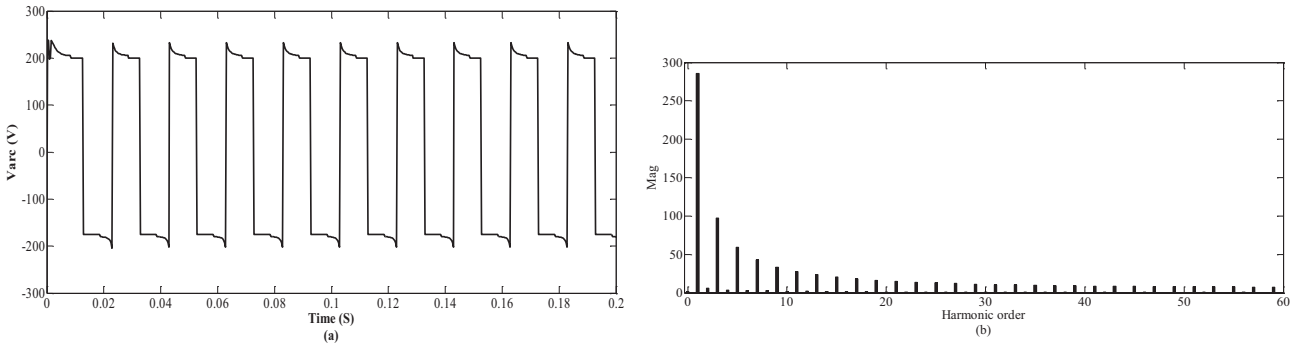

Figure 6. V_{arc} in the early stage of charging: (a) V_{arc}, (b) frequency spectrum of V_{arc}.

The obtained results and the frequency spectrum of the increased frequency signal are shown in Figure 7a and Figure 7b, respectively. As expected, the proposed method increases the frequency of all harmonics equal to half of the main frequency (25 Hz). The total harmonic distortion (THD) of the original signal and the increased frequency signal are 50.31% and 50.496%, respectively. The difference between these 2 THDs is due to the fact that the DC component in the original signal appears as a sinusoidal wave of 25 Hz frequency in the increased frequency signal.

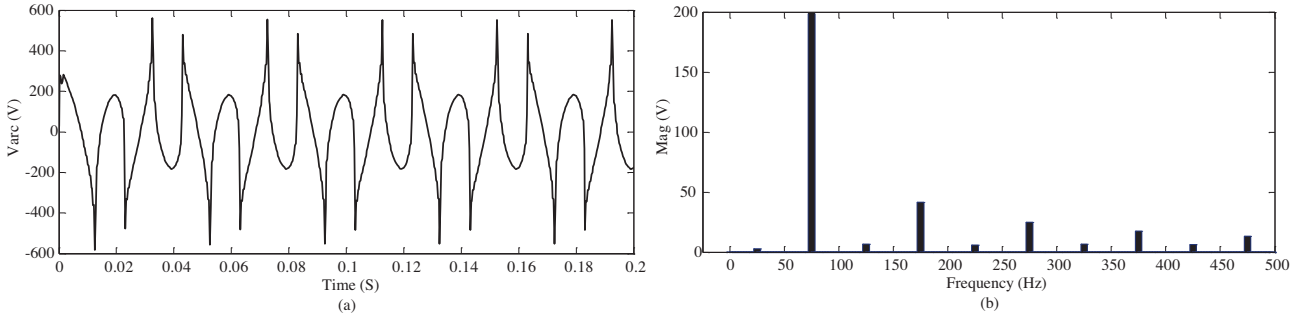

Figure 7. Frequency increased signal: (a) V_{arc}, (b) frequency spectrum of frequency increased signal.

5.1.3. Comparison with the conventional method

In this paper, 5 decomposition levels have been used in the conventional and the proposed methods. In the conventional method, the fundamental component of the input signal must be located at the center of the extracted frequency band. Therefore, the band width of the extracted frequency bands must be 100 Hz. On the other hand, the sampling frequency is equal to 6400 Hz in the conventional method. According to Eq. (4), the band width of 100 Hz can be achieved by 5 decomposition levels.

In the proposed method, the frequency of all harmonic components has been increased by half of the main frequency and the new frequencies are shown in Table 1.

Table 1. Frequency of harmonic components in the proposed method.

DC	1st	2nd	3rd	4th
25 Hz	75 Hz	125 Hz	175 Hz	225 Hz

According to Table 1, the band width of the extracted frequency bands must be 50 Hz to locate the harmonic components in the center of the extracted frequency bands. On the other hand, the sampling frequency is equal to 3200 Hz in the proposed method. Thus, according to Eq. (4), the band width of 50 Hz can be achieved by 5 decomposition levels.

As mentioned, the input signal is sampled so that the odd harmonics are located in the center of the extracted frequency bands in the conventional method. In this method, the even harmonics are located on the border of the extracted frequency bands, bringing about harmonic frequency interference. To address this issue, the first 4 extracted frequency bands in the conventional and proposed methods, as well as the harmonics present at each frequency band, are presented in Tables 2 and 3, respectively. According to Table 3, there are 2 harmonics on the border of each frequency band in the conventional method. Thus, there is always harmonic frequency interference between harmonic components. Moreover, the DC component is always located on the border of the first extracted frequency band while the calculation of the DC component amplitude is not included in the conventional method. However, in the proposed method, there is only 1 harmonic in each frequency band and no frequency interference takes place. Moreover, the calculation of the DC component amplitude is included.

Table 2. The extracted first 4 frequency bands in conventional and proposed methods.

Method	Sampling frequency (Hz)	Frequency band			
		d_5^0	d_5^1	d_5^2	d_5^3
Conventional	6400	0–100 Hz	100–200 Hz	200–300 Hz	300–400 Hz
Proposed	3200	0–50 Hz	50–100 Hz	100–150 Hz	150–200 Hz

Table 3. Extracted frequency bands and corresponding harmonics.

Method	Frequency band			
	d_5^0	d_5^1	d_5^2	d_5^3
Conventional	DC, 1st ,2nd	2nd , 3rd, 4th	4th, 5th, 6th	6th, 7th, 8th
Proposed	DC	1st	2nd	3rd

To calculate the RMS values, the selected sampling window width is ten cycles of the fundamental frequency (200 ms) as in IEC Standard 61000-4-30 [29]. The db43 is selected as the mother wavelet. In Section 7, the effect of different mother wavelets is evaluated. In the next subsections, the RMS values of V_{PCC} and V_{arc} are calculated in different operational conditions of the EAF by the conventional and proposed methods.

5.1.3.1. The early stage of charging

The absolute percentage errors for the RMS values of V_{arc} and V_{PCC} in the early stage of charging are presented in Figure 8a and Figure 8b, respectively. The results show that the absolute percentage errors in the conventional method are higher than those associated with the proposed method. The true RMS values of V_{PCC} and V_{arc} are listed in Table 4 as calculated by Fourier transform.

According to Table 4, the amplitudes of the DC component and the second harmonic are very low compared with the fundamental RMS value. Thus, the frequency interference is not clear enough in Figure 8. To examine the frequency interference in the conventional method, V_T of the negative current is decreased to 160. The true RMS values of V_{arc} and V_{PCC} are presented in Table 5 for this case. According to this table, the amplitude of the DC component and the 2nd harmonic are increased by 50% and 40%, respectively.

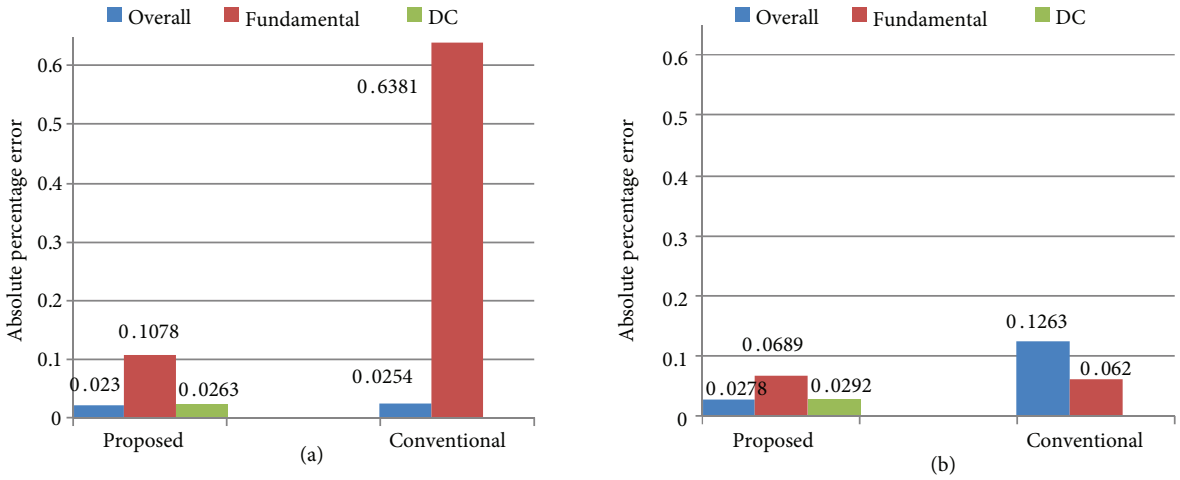

Figure 8. Absolute percentage errors of RMS values in the early stage of charging: (a) V_{arc}, (b) V_{PCC}.

Table 4. True RMS values of Varc and VPCC in the early stage of charging.

Voltage	DC component	Fundamental	2nd harmonic	Overall
V_{arc}	8.7307	182.8175	18.6959	205.3334
V_{PCC}	2.7405	284.3146	9.3833	288.1617

Table 5. True RMS values of Varc and VPCC in the early stage of charging.

Voltage	DC component	Fundamental	2nd harmonic	Overall
V_{arc}	13.0626	172.7105	26.2054	194.9405
V_{PCC}	4.0965	277.5786	13.1380	281.2272

The absolute percentage errors of the RMS values calculated by the proposed and conventional methods are presented in Figure 9a and Figure 9b. According to Figures 8 and 9, the absolute percentage errors in the conventional method increase with an increase in the amplitude of the DC component and the second harmonic while the accuracy of the proposed method is almost independent of the amplitudes of the second harmonic and DC component.

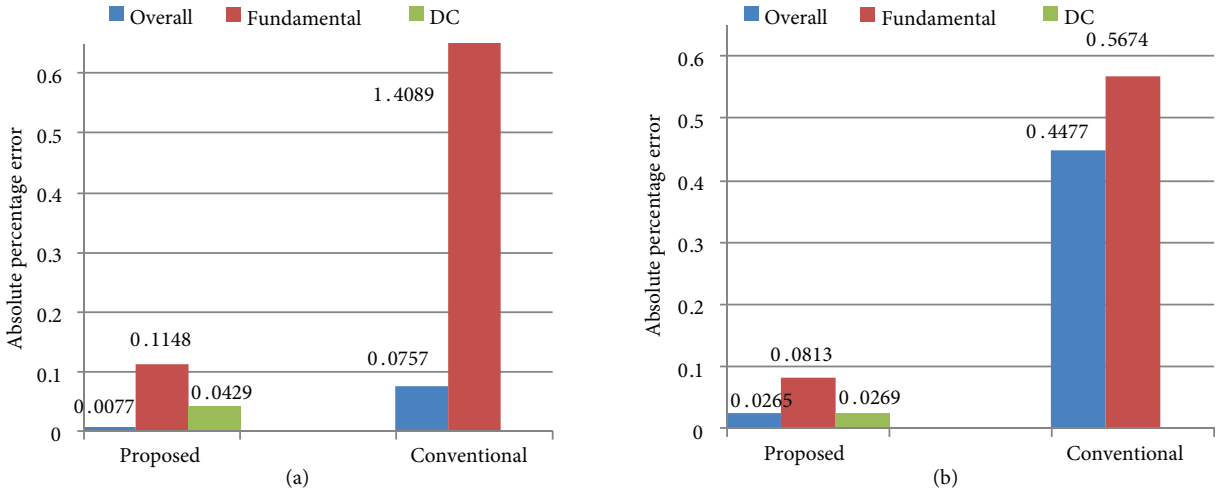

Figure 9. Absolute percentage errors of RMS values in the early stage of charging: (a) V_{arc}, (b) V_{PCC}.

5.1.3.2. Balanced condition

In this case, V_T in Eq. (17) is considered to be 220 for different phases as well as for the positive and negative currents. Thus, the EAF will work in the balanced condition. True RMS values of V_{arc} and V_{PCC} of phase a in the balanced condition and their absolute percentage errors are presented in Table 6, Figure 10a, and Figure 10b, respectively. As is clear from Table 6 and Figure 10, the absolute percentage errors associated with the proposed method are lower than in the conventional method for both the arc and PCC voltages due to the existence of the DC component and 2nd harmonic.

Table 6. True RMS values of Varc and VPCC of phase a in the balanced condition.

Voltage	DC component	Fundamental	2nd harmonic	Overall
V_{arc}	1.9701	202.0228	4.3628	225.9213
V_{PCC}	0.7697	297.4181	2.2132	301.7665

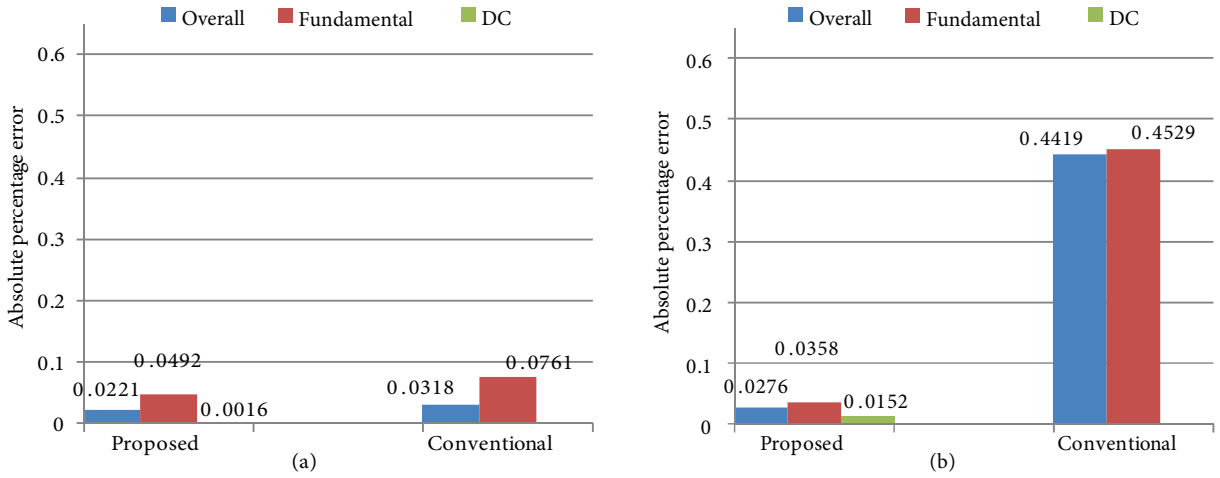

Figure 10. Absolute percentage errors of RMS values of phase a in the balanced condition: (a) V_{arc}, (b) V_{PCC}.

5.1.3.3. Unbalanced condition

In this case, V_T is considered to be different for different phases and the same for the positive and negative currents. V_T is considered to be 220, 250, and 280 for phases a, b, and c, respectively. The true RMS values of V_{arc} and V_{PCC} of phase b and phase c in the unbalanced condition and their absolute percentage errors are presented in Table 7 and Figures 11 and 12, respectively. The results obtained for phase a are the same as previously. Thus, the results are not presented for phase a. According to Figures 11 and 12, the accuracy of the proposed method is better than that of the conventional method, especially for VPCC. However, for V_{arc}, the accuracy of the conventional method for the fundamental RMS is slightly better than that of the proposed method due to the low amplitudes of the DC component and 2nd harmonics. Moreover, the accuracy of the proposed method for the overall RMS is slightly better than that of the conventional method.

5.1.4. Comparison with the grouping method

In this subsection, the proposed method is compared with the grouping method in terms of accuracy. In order to address this issue, V_{arc} and V_{PCC} are sampled at 3200 Hz and 5 decomposition levels are considered. The db43 has been selected as the mother wavelet in both methods.

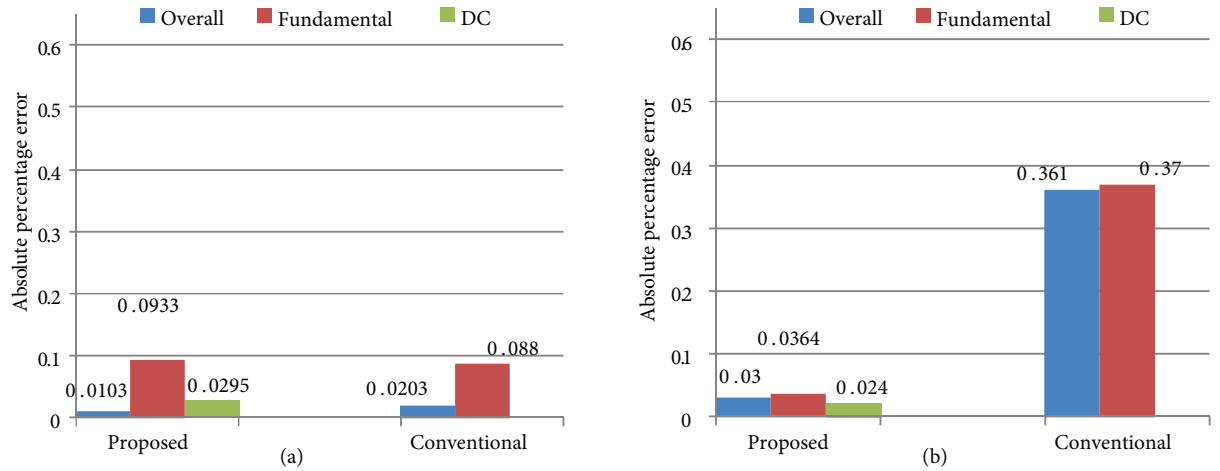

Figure 11. Absolute percentage errors of RMS values in unbalanced condition for phase b: (a) V_{arc}, (b) V_{PCC}.

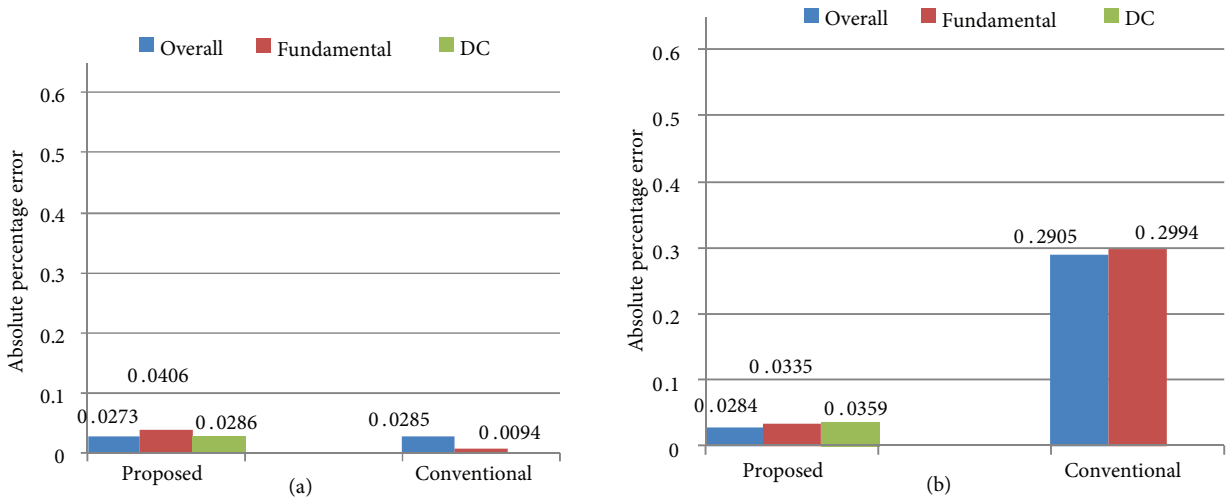

Figure 12. Absolute percentage errors of RMS values in unbalanced condition for phase c: (a) V_{arc}, (b) V_{PCC}.

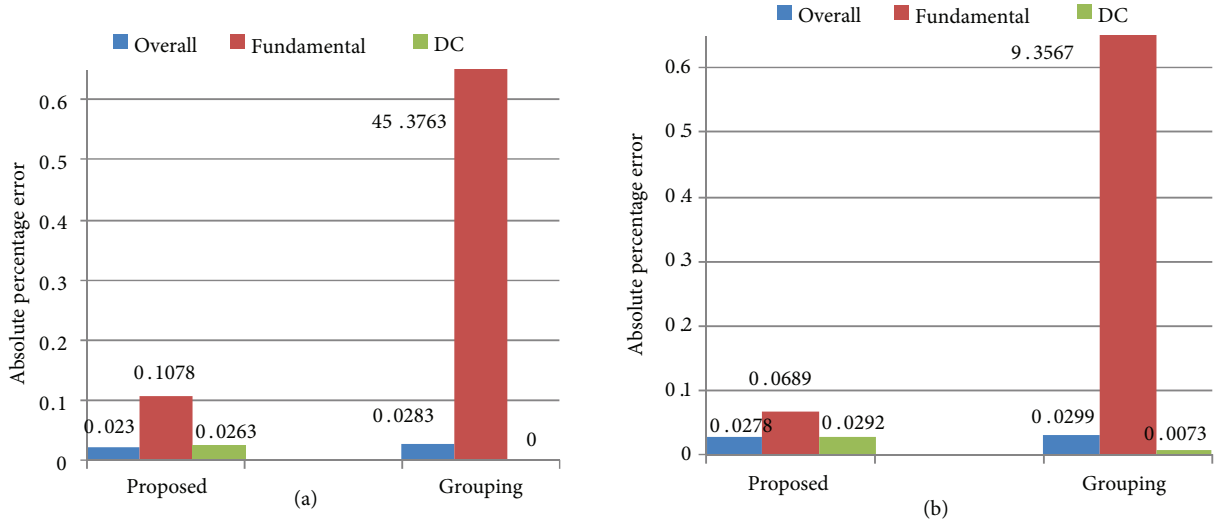

Figure 13. Absolute percentage errors of RMS values in the early stage of charging: (a) V_{arc}, (b) V_{PCC}.

In the grouping method, only one harmonic must exist at the borders of each extracted frequency band. Thus, the band width of the extracted frequency bands should be 25 Hz. Therefore, according to Eq. (4), the number of wavelet levels must be 6 to obtain the band width of 25 Hz.

Figures 13 and 14 present the absolute percentage errors of the RMS values for V_{arc} and V_{PCC} in the early stage of charging and balanced conditions, respectively. Moreover, Figures 15 and 16 present the absolute percentage errors of RMS values for V_{arc} and V_{PCC} in the unbalanced conditions. According to these figures, the fundamental RMS values presented by the grouping method are not acceptable because of their high errors. However, the DC components are calculated with very high accuracy by the grouping method such that the errors associated with the DC component are zero in most cases. For the overall RMS values, the results obtained by both proposed and grouping methods are calculated with high accuracy, but the accuracy of the overall RMS values of the proposed method is slightly better than that of the grouping method.

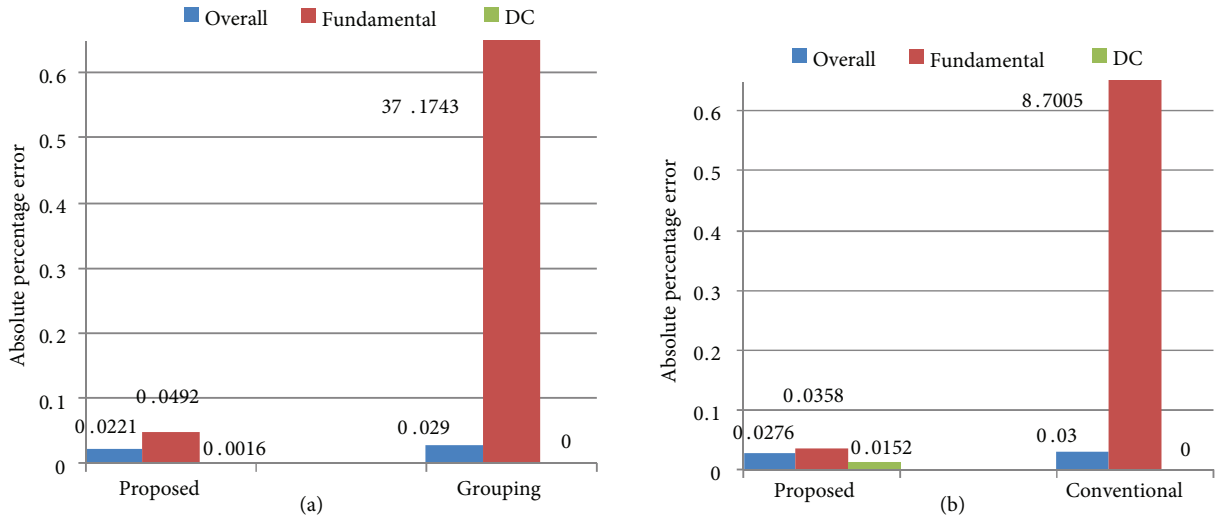

Figure 14. Absolute percentage errors of RMS values in balanced condition for phase a: (a) V_{arc}, (b) V_{PCC}.

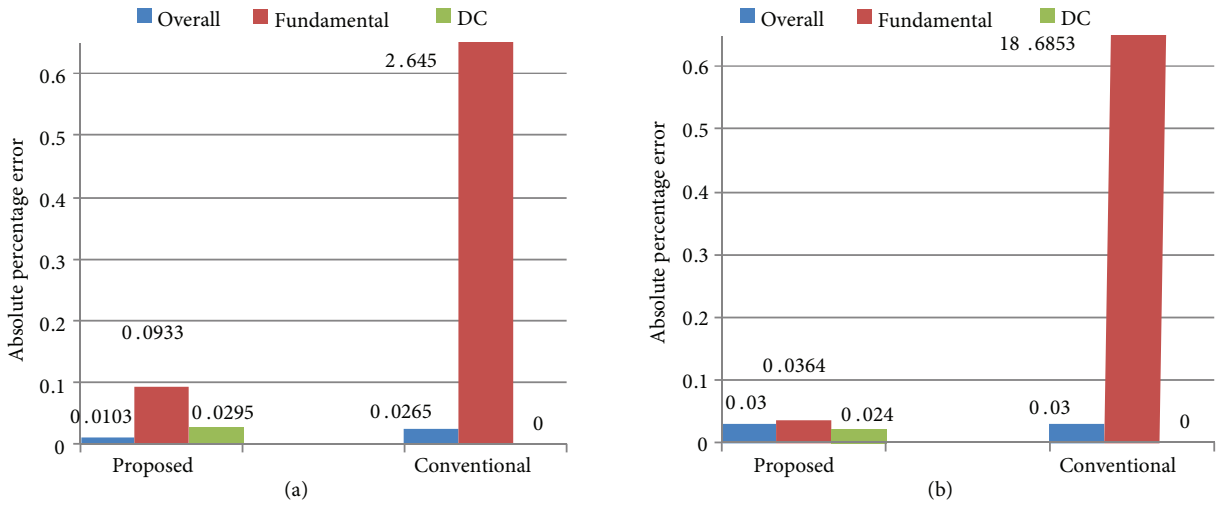

Figure 15. Absolute percentage errors of RMS values in unbalanced condition for phase b: (a) V_{arc}, (b) V_{PCC}.

5.2. Second case study (hypothetical signal)

In this case, a hypothetical signal with different types of harmonics is simulated in MATLAB software to evaluate the performance of the 3 above-mentioned methods. At first, a signal with only odd harmonics is simulated as follows:

$$x(t) = 100\sin(\omega t) + 40\sin(3\omega t) + 30\sin(5\omega t), \omega = 100\pi \tag{18}$$

In Figure 17, the absolute percentage errors for 3 methods are shown in the case with only odd harmonics. According to this figure, the conventional method has the best performance because of the absence of even harmonics (no frequency interference) and the absolute percentage error associated with the fundamental is very high in the grouping method. Moreover, the absolute percentage error associated with the overall RMS value is the same in the methods.

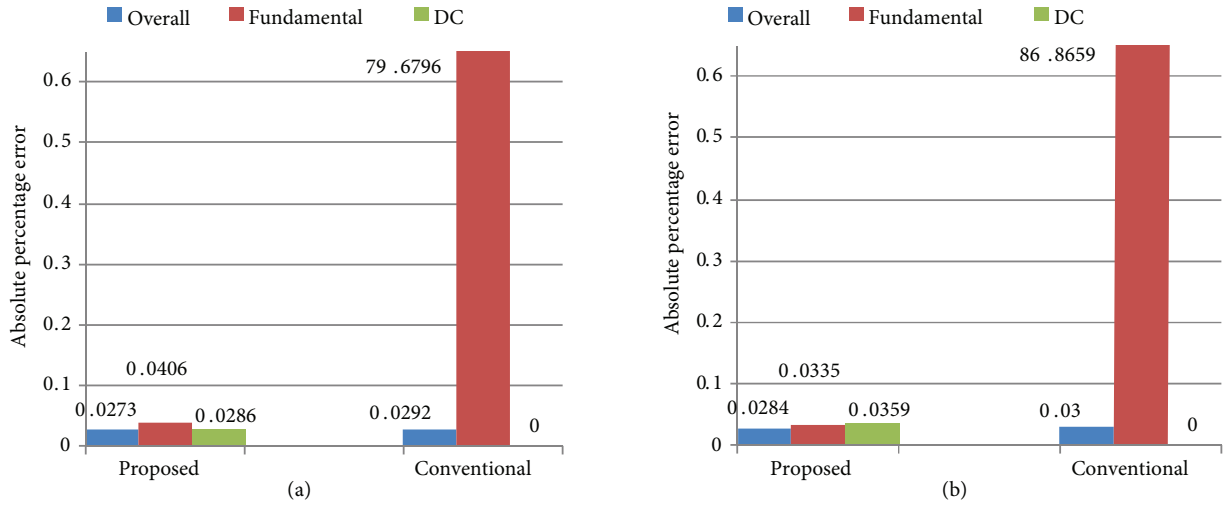

Figure 16. Absolute percentage errors of RMS values in unbalanced condition for phase c: (a) V_{arc}, (b) V_{PCC}.

To examine the effect of the DC component on the accuracy of the methods, a DC component with amplitude of 5 is added to the simulated signal in Eq. (18).

$$x(t) = 100\sin(\omega t) + 40\sin(3\omega t) + 30\sin(5\omega t) + 5 \tag{19}$$

In this case, the proposed method has the best performance as shown in Figure 18 and because of the frequency interference phenomena, the absolute percentage error associated with the fundamental RMS increases in the conventional method.

To consider the odd and even harmonics and the DC component simultaneously, the even harmonics are added to the hypothetical signal in Eq. (19).

$$x(t) = 100\sin(\omega t) + 20\sin(2\omega t) + 40\sin(3\omega t) + 10\sin(4\omega t) + 30\sin(5\omega t) + 5 \tag{20}$$

As it shown in Figure 19, the accuracy of the overall RMS is the same for the 3 methods. However, the accuracy of the fundamental RMS for the proposed method is far better than that of the other 2 methods. Moreover, the accuracy of the DC component calculation in the grouping method is better than that of the proposed method.

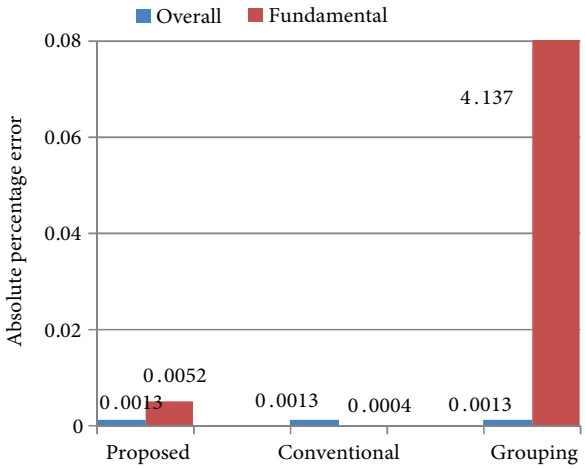

Figure 17. Absolute percentage errors of RMS values for hypothetical signal with only odd harmonics.

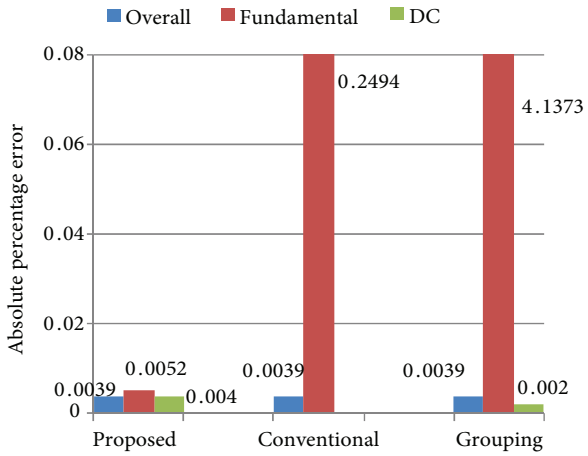

Figure 18. Absolute percentage errors of RMS values for hypothetical signal with odd harmonics and DC component.

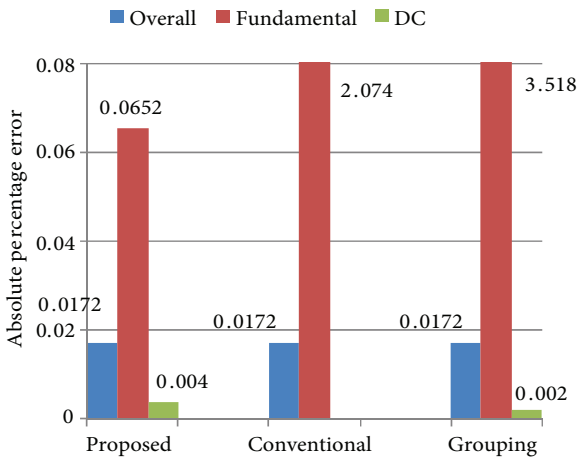

Figure 19. Absolute percentage errors of RMS values for hypothetical signal with odd and even harmonics and DC component.

6. Time cost and computational burden

The time cost of the traditional and the proposed methods is shown in Table 8. The calculations are performed by MATLAB 2010a on an Intel core i5 2.53 GHz with a memory of 4.00 GB.

Table 8. Time cost of the methods.

Method	Time cost
Proposed	0.956905 s
Conventional	0.961312 s
Grouping	1.376785 s

According to Table 8, the time cost of the proposed and the conventional methods is almost the same, but the time cost of the grouping method is higher than that of the proposed and the conventional methods.

Two factors affecting the time cost are the sampling frequency and the number of wavelet levels. The number of the wavelet levels is the same in both the proposed and the conventional methods, but the sampling frequency in the conventional method is higher than that of the proposed method. Higher sampling frequency increases the number of samples leading to higher time cost. Therefore, the conventional method requires a little more time than the proposed method.

As shown in Figure 3, each extracted frequency band requires a certain amount of computation. Thus, if the extracted frequency bands are increased, the computational burden will also increase. The WPT levels required for the proposed and the conventional methods are less than those for the grouping method. If the number of the WPT levels in the grouping method is equal to N, the number of the WPT levels in the proposed and the conventional methods will be equal to $N - 1$. Therefore, the difference between the numbers of the extracted frequency bands is expressed according to Eq. (6) as follows.

$$\Delta M = M_{GroupingMethod} - M_{\mathrm{Pr}\,oposedMethod} = 2^N \tag{21}$$

According to Eq. (21), the grouping method has 2^N more extracted frequency bands than the proposed and the conventional methods. For example, in this paper, 6 decomposition levels were used in the grouping method. Therefore, the grouping method has 64 more extracted frequency bands than the proposed and the conventional methods, requiring more time than the proposed and the conventional methods.

7. Effect of mother wavelet

There are many mother wavelets that can be used for signal analysis. In this paper, the effect of Daubechies (db), biorthogonal (BIOR), reverse biorthogonal (RBIOR), and Coiflet (COFI) mother wavelets are evaluated based on the accuracy of the RMS values. In Figure 20, the absolute percentage errors of RMS values of V_{PCC} calculated by different mother wavelets are provided. According to this figure, among the Daubechies mother wavelets, the db43, db35, and db30 mother wavelets provide acceptable results and the db43 mother wavelet has the best performance. The other mother wavelets provide great errors, especially for the DC component. Thus, the db43 mother wavelet is the best candidate for the RMS value calculation.

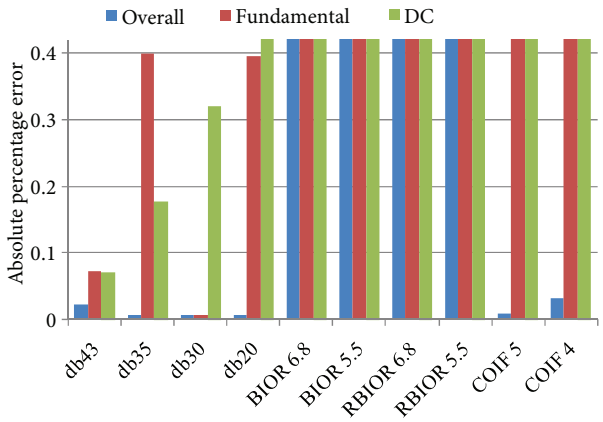

Figure 20. Effect of mother wavelets on RMS values calculation accuracy.

The db43 mother wavelet, which is a 43-order mother wavelet, is a member of the Daubechies mother wavelet family. The Daubechies mother wavelet family contains many mother wavelets. The waveforms of different Daubechies mother wavelets are shown in Figure 21 [30]. As can be seen from this figure, as the

order of Daubechies mother wavelets is increased, the mother wavelet becomes more complex. Increasing the mother wavelet order increases the calculation accuracy, but higher order than 43 brings about instability in the algorithm used for the computation of the mother wavelet coefficient [7].

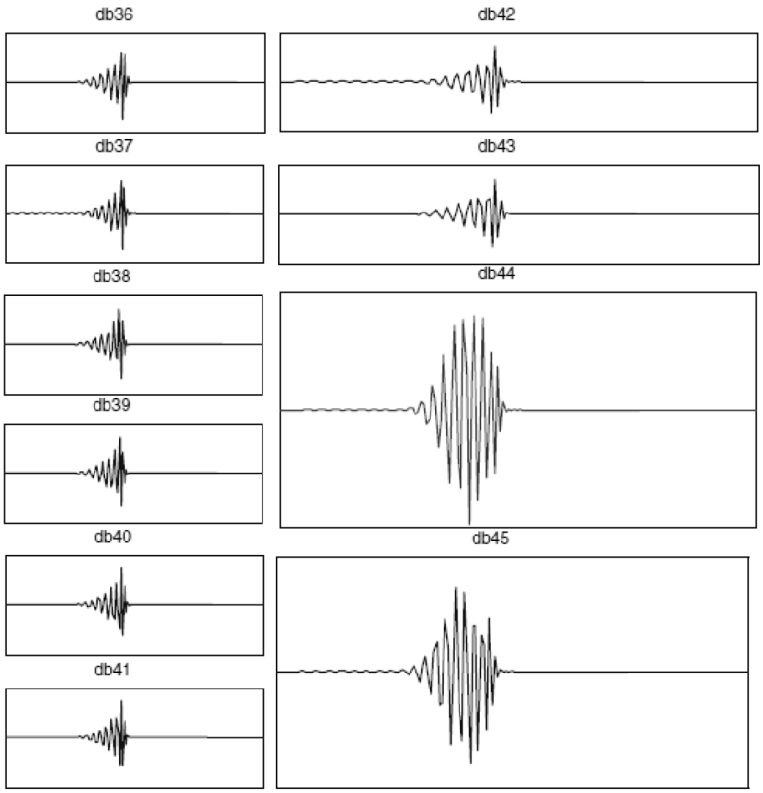

Figure 21. Waveform of the differently ordered Daubechies mother wavelets [25].

8. Conclusion

In this paper, a new combined method was proposed based on WPT and Hilbert transform for RMS value calculation. The proposed method increases the frequency of all the components equal to half of the main frequency. Thus, the frequency of all the components is located in the center of the extracted frequency bands and the accuracy of RMS value calculation is enhanced. To evaluate the proposed method and consider both odd and even harmonics, the supply network of the EAF of the EMSC and a hypothetical signal were simulated in MATLAB software. The proposed method was compared with the conventional and grouping methods and the results showed that the proposed method, unlike the conventional and grouping methods, could calculate the fundamental RMS value more accurately. Furthermore, the number of extracted frequency bands by the proposed method was less than in the grouping method.

References

[1] Hooshmand RA, Banejad M, Esfahani MT. A new time domain model for electric arc furnace. Journal of Electrical Engineering 2008; 59: 195-202.

[2] Hajibeigy M, Farsadi M. Harmonic suppression in HVDC system using a modified control method for hybrid active DC filter. Eur T Electr Power 2012; 22: 294-307.

[3] Sutinko T, Jidin A, Idrist NRN. New approach FPGA-based implementation of discontinuous SVPWM. Turk J Electr Eng Co 2010; 18: 499-514.

[4] Hooshmand RA, Noohi S. Neural network-based algorithm for harmonic analysis of industrial systems using asynchronous simulations in time and frequency domains. IEEJ T Electr Electr 2010; 5: 688-694.

[5] Saxena D, Bhaumik S, Singh SN. Identification of multiple harmonic sources in power system using optimally placed voltage measurement devices. IEEE T Ind Electron 2014; 61: 2483-2492.

[6] Allenbaugh ML, Dionise TJ, Natali TJ. Harmonic analysis and filter bank design for a new rectifier for a cold roll mill. IEEE T Ind Appl 2013; 49: 1161-1170.

[7] Morsi WG, El-Hawary ME. A new reactive, distortion and non-active power measurement method for nonstationary waveforms using wavelet packet transform. Electr Pow Syst Res 2009; 79: 1408-1415.

[8] Jain SK, Singh SN. Fast harmonic estimation of stationary and time-varying signals using EA-AWNN. IEEE T Instrum Meas 2013; 62: 335-343.

[9] Akinci TC, Ekren N, Seker S, Yildirim S. Continuous wavelet transform for ferroresonance phenomena in electric power systems. Int J Elec Power 2013; 44: 403-409.

[10] Vatansever F, Ozdemir A. A new approach for measuring RMS value and phase angle of fundamental harmonic based on wavelet packet transform. Electr Pow Syst Res 2008; 78: 74-79.

[11] Ren J, Kezunovic M. Real-time power system frequency and phasors estimation using recursive wavelet transform. IEEE T Power Deliver 2011; 26: 1392-1402.

[12] Morsi WG, El-Hawary ME. Time-frequency single-phase power components measurements for harmonics and inter-harmonics distortion based on wavelet packet transform; Part II: case studies and results. Can J Elect Comput E 2010; 35: 8-14.

[13] Nath S, Sinha P, Goswami SK. A wavelet based novel method for the detection of harmonic sources in power systems. Int J Elec Power 2012; 40: 54-61.

[14] Barros J, Diego RI. Analysis of harmonics in power systems using the wavelet-packet transform. IEEE T Instrum Meas 2008; 57: 63-69.

[15] Diego RI, Barros J. Global method for time–frequency analysis of harmonic distortion in power systems using the wavelet packet transform. Electr Pow Syst Res 2009; 79: 1226-1239.

[16] Diego RI, Barros J. Subharmonic measurement using DFT and wavelet-packet transform in an IEC extended framework. Measurement 2010; 43: 1603-1608.

[17] Barros J, Diego ROI. A new method for measurement of harmonic groups in power systems using wavelet analysis in the IEC standard framework. Electr Pow Syst Res 2006; 76: 200-208.

[18] Barros J, Diego RI. Application of the wavelet-packet transform to the estimation of harmonic groups in current and voltage waveforms. IEEE T Power Deliver 2006; 21: 533-535.

[19] Barros J, Diego RI, Apraiz MD. A discussion of new requirements for measurement of harmonic distortion in modern power supply systems. IEEE T Instrum Meas 2013; 62: 2129-2139.

[20] Morsi WG, Diduch CP, Chang L, El-Hawary ME. Wavelet-based reactive power and energy measurement in the presence of power quality disturbances. IEEE T Power Syst 2011; 26: 1263-1271.

[21] Chen Y. Harmonic detection in electric power system based on wavelet multi-resolution analysis. In: International Conference on Computer Science and Software Engineering; 2008. pp. 1204-1207.

[22] Vatansever F, Ozdemir A. Power parameters calculations based on wavelet packet transform. Int J Elec Power 2009; 31: 596-603.

[23] Ferretti M, Rizzo D. Handling borders in systolic architectures for the 1-D discrete wavelet transform for perfect reconstruction. IEEE T Signal Proces 2000; 48: 1365-1378.

[24] Su H, Liu Q, Li J. Boundary effects reduction in wavelet transform for time-frequency analysis. WSEAS Transactions on Signal Processing 2012; 8: 169-179.

[25] Dehkordi BM, Parsapoor A, Hooshmand R. Effect of different operating conditions of electric arc furnace on synchronous generator shaft. In: International Aegean Conference on Electrical Machines and Power Electronics; 2007. pp. 824-829.

[26] Golkar MA, Bina MT, Meschi S. A novel method of electrical arc furnace modeling for flicker study. In: International Conference on Renewable Energies and Power Quality; 2007. pp. 1-8.

[27] Bhonsle DC, Kelkar RB. Design and analysis of composite filter for power qualify improvement of electric arc furnace. In: International Conference on Electric Power and Energy Conversion Systems; 2013. pp. 1-10.

[28] Bhonsle DC, Kelkar RB. Simulation of electric arc furnace characteristics for voltage flicker study using MATLAB. In: International Conference on Recent Advancements in Electrical, Electronics and Control Engineering; 2011. pp. 174-181.

[29] IEC. Electromagnetic Compatibility (EMC), Pt. 4, Section 30: Power Quality Measurement Methods, IEC 61000-4-30.

[30] Rafiee J, Rafiee MA, Prause N, Schoen MP. Wavelet basis functions in biomedical signal processing. Expert Syst Appl 2011; 38: 6190-6201.

A. Appendix

The RMS value of $v(t)$ is provided by the following equation in the time domain.

$$v_{rms} = \sqrt{\frac{1}{T}\int_0^T v^2(t)\,dt} \tag{A.1}$$

If Eq. (7) is substituted into Eq. (A.1):

$$v_{rms} = \sqrt{\frac{1}{T}\int_0^T \left[\sum_{k=0}^{2^{N-j}-1} d_j^0[k]\,\phi_{j,k}(t) + \sum_{m=1}^{2^j-1}\left(\sum_{k=0}^{2^{N-j}-1} d_j^m[k]\,\psi_{j,k}^m(t)\right)\right]^2 dt} \tag{A.2}$$

Since $(a+b)^2 = a^2 + 2ab + b^2$, we have:

$$v_{rms} = \sqrt{\frac{1}{T}\left\{\begin{array}{l}\sum_{k=0}^{2^{N-j}-1}\left[d_j^0[k]\right]^2\int_0^T\left[\phi_{j,k}(t)\right]^2 dt + 2\sum_{m=1}^{2^j-1}\left(\sum_{k=0}^{2^{N-j}-1} d_j^0[k]\,d_j^m[k]\right)\int_0^T \phi_{j,k}(t)\,\psi_{j,k}^m(t)\,dt \\ +\sum_{m=1}^{2^j-1}\left(\sum_{k=0}^{2^{N-j}-1}\left[d_j^m[k]\right]^2\psi_{j,k}^m(t)\int_0^T\left[\psi_{j,k}^m(t)\right]^2 dt\right)\end{array}\right\}} \tag{A.3}$$

If the following properties of wavelets are used:

$$\int_0^T\left[\phi_{j,k}(t)\right]^2 dt = 1,\ \int_0^T \phi_{j,k}(t)\,\psi_{j,k}^m(t)\,dt = 0,\ \int_0^T\left[\psi_{j,k}^m(t)\right]^2 dt = 1 \tag{A.4}$$

And if Eq. (A.4) is substituted into Eq. (A.3):

$$v_{rms} = \sqrt{\frac{1}{T}\left\{\sum_{k=0}^{2^{N-j}-1}\left(d_j^0[k]\right)^2 + \sum_{m=1}^{2^j-1}\left(\sum_{k=0}^{2^{N-j}-1}\left(d_j^m[k]\right)^2\right)\right\}} \tag{A.5}$$

If this relationship is written in discrete form, we have the following equation, from which Eq. (8) is obtained:

$$v_{rms} = \sqrt{\frac{1}{2^N}\sum_{k=0}^{2^{N-j}-1}\left(d_j^0[k]\right)^2 + \frac{1}{2^N}\sum_{m=1}^{2^j-1}\left(\sum_{k=0}^{2^{N-j}-1}\left(d_j^m[k]\right)^2\right)} \tag{A.6}$$

B. Appendix

This appendix describes the parameters used in simulations as shown in Figure 5. These parameters are shown in Tables B1 and B2.

Table 1B. Specifications of the supplying network of EAF of EMSC.

X_t (mΩ)	R_t (mΩ)	$\dot{X}_{SC}$ (mΩ)	$\dot{R}_{SC}$(mΩ)	f (Hz)	E_{AC} (V)
7.867	1.899	7.976	0.8524	50	586